A spin-liquid with pinch-line singularities on the pyrochlore lattice

Owen Benton, L. D.C. Jaubert, Han Yan, Nic Shannon

▶ **To cite this version:**

Owen Benton, L. D.C. Jaubert, Han Yan, Nic Shannon. A spin-liquid with pinch-line singularities on the pyrochlore lattice. Nature Communications, 2016, 7, pp.11572. 10.1038/ncomms11572 . hal-01542093

HAL Id: hal-01542093
https://hal.science/hal-01542093

Submitted on 21 Jun 2017

HAL is a multi-disciplinary open access archive for the deposit and dissemination of scientific research documents, whether they are published or not. The documents may come from teaching and research institutions in France or abroad, or from public or private research centers.

L'archive ouverte pluridisciplinaire **HAL**, est destinée au dépôt et à la diffusion de documents scientifiques de niveau recherche, publiés ou non, émanant des établissements d'enseignement et de recherche français ou étrangers, des laboratoires publics ou privés.

From pinch points to pinch lines: a new spin liquid on the pyrochlore lattice

Owen Benton,[1] L. D. C. Jaubert,[1] Han Yan,[1] and Nic Shannon[1]

[1]*Okinawa Institute of Science and Technology Graduate University, Onna-son, Okinawa 904-0395, Japan*

The mathematics of gauge theories lies behind many of the most profound advances in physics in the last 200 years, from Maxwell's theory of electromagnetism to Einstein's theory of general relativity. More recently it has become clear that gauge theories also emerge in condensed matter, a prime example being the "spin ice" materials which host an emergent "electromagnetic" gauge field. In spin ice, the underlying gauge structure is revealed by the presence of "pinch-point" singularities in neutron-scattering measurements. Here we report the discovery of a new spin liquid where the low-temperature physics is naturally described by the fluctuations of a tensor field with a continuous gauge freedom. This gauge structure underpins a novel form of spin correlations, giving rise to "pinch-line" singularities — line-like analogues of the pinch-points observed in spin ice. Remarkably, these features may already have been observed in the pyrochlore material $Tb_2Ti_2O_7$.

Gauge symmetries are paramount in the understanding of many of the most fundamental theories of physics. Recent decades have seen an increasing appreciation of the role of gauge theories in condensed matter physics, emerging from the long-wavelength description of the collective behaviour of electrons. Emergent gauge theories have proved particularly important in the study of spin liquids – strongly fluctuating, disordered magnetic states, the description of which lies beyond the familiar territory of Landau theory [1–5].

The use of a gauge theory to describe the fluctuations of a spin liquid is exemplified by the case of the spin ice materials $R_2M_2O_7$ (R=Ho, Dy, M=Ti, Sn) [6, 7]. At low temperatures, the spin configurations in a spin ice are subject to a constraint directly analogous to Gauss' law for a magnetic field and consequently may be described in terms of a gauge theory. Among the many striking consequences of this is the observation of pinch-point singularities [Fig. 1(a), left panel] in the magnetic neutron scattering structure factor [8], as observed in $Ho_2Ti_2O_7$ [9]. Pinch-point scattering has also been observed in the putative quantum spin ice $Tb_2Ti_2O_7$ [10–12]. However, in this case the experimental scattering shows pronounced butterfly-like features in the non spin-flip (NSF) channel and the scattering in the spin-flip (SF) channel shows narrow arm-like features extending along the $\langle 111 \rangle$ directions of reciprocal space, neither of which features are predicted for a spin ice. This raises the question of whether other types of spin liquid may be found amongst rare-earth pyrochlore magnets.

In this Article we introduce a new type of spin liquid on the pyrochlore lattice. This spin liquid arises on the phase diagram of a realistic model for pyrochlore magnets. As with spin ice, the theory of this spin liquid contains a gauge symmetry. The nature of this theory is fundamentally different to the Maxwellian theory which describes spin ice, but just as the emergent gauge structure of spin ice reveals itself in pinch-point scattering, so the gauge structure of this new spin liquid has striking consequences for scattering experiments. We will show that at low temperatures, this gauge structure leads to line-like singularities along the $\langle 111 \rangle$ directions of reciprocal space, which we dub "pinch lines" since they are extended versions of the pinch points exhibited in spin ice. This is particularly interesting in the light of neutron scattering results on the pyrochlore magnets $Tb_2Ti_2O_7$ and $Yb_2Ti_2O_7$ which show strong, sharpening features along the $\langle 111 \rangle$ directions of reciprocal space. Indeed, our theory is able to account for several features of the diffuse scattering observed in $Tb_2Ti_2O_7$ [10–12], which are unaccounted for by a theory based on a spin ice model — as shown in the right panels of Fig. 1.

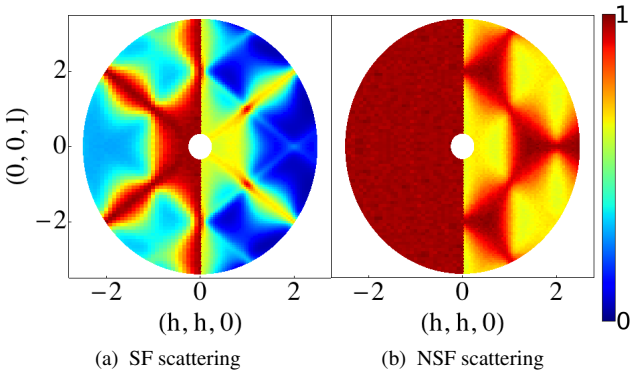

(a) SF scattering (b) NSF scattering

FIG. 1: **Comparison of correlations in spin ice (left half of panels) with those of the new spin liquid (right half of panels).** Predictions for polarised neutron scattering experiments are shown in the (a) spin–flip (SF) and (b) non spin–flip (NSF) channels, as measured by Fennell *et al.* [9, 10]. The prediction for spin ice exhibits pinch–point singularities in the SF channel. The NSF channel is completely featureless in a nearest neighbour model for spin ice–as shown here–and develops smooth maxima at the zone boundaries in the presence of long range dipole interactions [9]. In contrast, the new spin liquid exhibits singular features in both SF and NSF scattering. Results are taken from classical Monte Carlo simulation of the nearest neighbour model $\mathcal{H}_{\rm ex}$ [Eq. (1)], as described in the text.

Results

We begin with the most general, symmetry-allowed, Hamiltonian for nearest neighbour anisotropic exchange on the py-

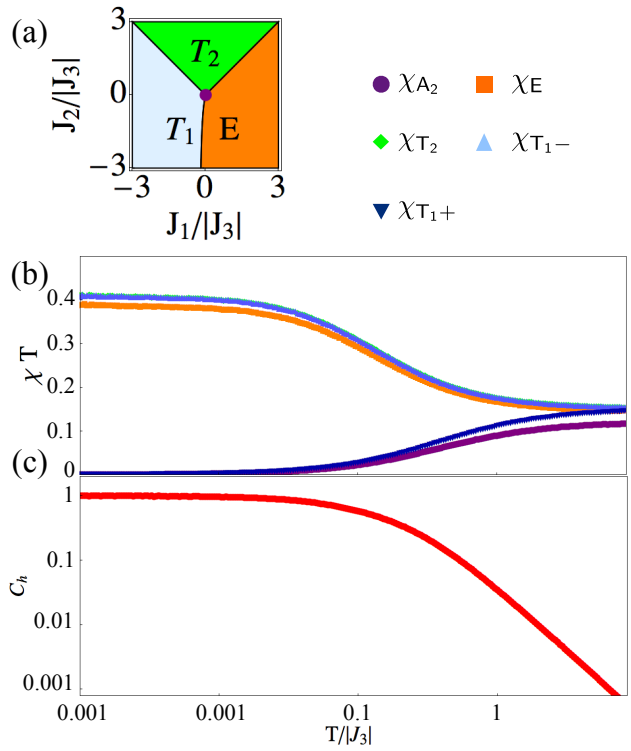

FIG. 2: **Evidence of spin–liquid behaviour from Monte Carlo simulation**. (a) Classical ground state phase diagram of $\mathcal{H}_{\rm ex}$ [Eq. (1)] for $J_3{<}0$, in the plane $J_4{=}0$, showing how ordered phases with symmetry T_1, E and T_2 meet at the point $J_1{=}J_2{=}0$ [15]. (b) Order–parameter susceptibilities and (c) heat capacity calculated in classical Monte Carlo simulation of $\mathcal{H}_{\rm ex}$ [Eq. (1)], for parameters $J_1{=}J_2{=}J_4{=}0$, $J_3 < 0$. No phase transition is observed down to $T = 0.001|J_3|$. Instead, the order parameter susceptibilities of neighbouring ordered phases exhibit a Curie–law crossover, characteristic of a Coulombic spin liquid [18]. The symbols used for different symmetry channels are shown in an inset.

rochlore lattice [13–15]:

$$\mathcal{H}_{\rm ex} = \sum_{\langle ij \rangle} \mathbf{S}_i \cdot \bar{\mathcal{J}}_{ij} \cdot \mathbf{S}_j \ , \qquad \bar{\mathcal{J}}_{01} = \begin{pmatrix} J_2 & J_4 & J_4 \\ -J_4 & J_1 & J_3 \\ -J_4 & J_3 & J_1 \end{pmatrix} \quad (1)$$

where the exchange matrix $\bar{\mathcal{J}}_{01}$ couples nearest neighbours along the $\mathbf{r}_{01} = (0,1,1)$ direction and the other exchange matrices can be generated from $\bar{\mathcal{J}}_{01}$ using point group operations. As shown in [15, 16], it is possible to map out the entire classical ground state phase diagram of Eq. (1) by an exact transcription of the Hamiltonian in terms of local fields defined on each tetrahedron [15–17]:

$$\mathcal{H}_{\rm ex} = \frac{1}{2} \sum_{\rm tet} \Big[\Delta_{\mathsf{A}_2} m_{\mathsf{A}_2}^2 + + \Delta_{\mathsf{E}} \mathbf{m}_{\mathsf{E}}^2 + \Delta_{\mathsf{T}_2} \mathbf{m}_{\mathsf{T}_2}^2 + \Delta_{\mathsf{T}_1-} \mathbf{m}_{\mathsf{T}_1-}^2 + \Delta_{\mathsf{T}_1+} \mathbf{m}_{\mathsf{T}_1+}^2 \Big] + E_0 \quad (2)$$

where all the coefficients $\Delta_\alpha \geq 0$, E_0 is the ground state energy and the sum runs over all tetrahedra in the lattice.

The five fields $m_{\mathsf{A}_2}, \mathbf{m}_{\mathsf{E}}, \mathbf{m}_{\mathsf{T}_2}, \mathbf{m}_{\mathsf{T}_1-}, \mathbf{m}_{\mathsf{T}_1+}$ appearing in Eq. (2) are defined in the supplemental material. They transform according to the $\mathsf{A}_2, \mathsf{E}, \mathsf{T}_2, \mathsf{T}_1$ irreducible representations of the point group and have respective dimension $1, 2, 3, 3$ and 3. Along a line of points in parameter space the three ordered phases which respectively maximise the fields $\mathbf{m}_{\mathsf{T}_1-}, \mathbf{m}_{\mathsf{T}_2}, \mathbf{m}_{\mathsf{E}}$ become degenerate. This line includes the point $J_1 = J_2 = J_4 = 0, J_3 < 0$ [cf. Fig. 2(a)]. For parameter sets along this line of points we have $\Delta_{\mathsf{A}_2} = \Delta_{\mathsf{E}} = \Delta_{\mathsf{T}_1-} = 0, \Delta_{\mathsf{A}_2}, \Delta_{\mathsf{T}_1+} > 0$ and the Hamiltonian is given by

$$\mathcal{H}_{\rm ex}^{\rm CL} = \frac{1}{2} \sum_{\rm tet} [\Delta_{\mathsf{A}_2} m_{\mathsf{A}_2}^2 + \Delta_{\mathsf{T}_1+} \mathbf{m}_{\mathsf{T}_1+}^2] + E_0. \quad (3)$$

In a classical ground state of Eq. (3) it must be the case that

$$m_{\mathsf{A}_2} = 0, \qquad \mathbf{m}_{\mathsf{T}_1+} = 0 \quad (4)$$

for every tetrahedron in the lattice. All of the results derived in this paper flow from the implementation of these constraints. These provide an exact description of the classical ground states along the line in parameter space where the three phases in Fig. 2(a) are degenerate. Observing the consequences of these constraints does not, however, require precise fine tuning of the Hamiltonian to Eq. (3). These constraints will also dominate the physics at finite temperatures for any choice of parameters where $\Delta_{\mathsf{A}_2}, \Delta_{\mathsf{E}}, \Delta_{\mathsf{T}_1-} << \Delta_{\mathsf{A}_2}, \Delta_{\mathsf{T}_1+}$ such that energy cost of having a finite value of the fields $\mathbf{m}_{\mathsf{T}_1-}, \mathbf{m}_{\mathsf{T}_2}, \mathbf{m}_{\mathsf{E}}$ is much lower than the cost to have a finite value of $m_{\mathsf{A}_2}, \mathbf{m}_{\mathsf{T}_1+}$.

The constraints in Eq. 4 are insufficient to select an ordered ground state in themselves. In such circumstances, fluctuations may select a preferred ordered state via the order–by–disorder mechanism, but Monte Carlo simulations indicate that they fail to do so, down to temperatures 3 orders of magnitude below the scale of the bare coupling [see Fig. 2(b)]. The system thus remains in a disordered but highly-correlated state down to low temperature.

We can understand the correlations of the spin liquid from Eq. (4). The demand that the fields m_{A_2} and $\mathbf{m}_{\mathsf{T}_1+}$ vanish everywhere leaves the fields $\{\mathbf{m}_{\mathsf{E}}, \mathbf{m}_{\mathsf{T}_2}, \mathbf{m}_{\mathsf{T}_1-}\}$ with freedom to fluctuate in the ground state. The spatial variation of these fluctuations is constrained by the fact that neighbouring tetrahedra share a spin, therefore a fluctuation of the local fields on one tetrahedron affects the values of the local fields on the neighbouring tetrahedra. The fields $\mathbf{m}_{\mathsf{E}}, \mathbf{m}_{\mathsf{T}_2}, \mathbf{m}_{\mathsf{T}_1-}$ must therefore fluctuate in a correlated manner in order to avoid inducing violations of Eq. (4). In what follows we show how these correlated fluctuations can be understood in terms of the fluctuations of a tensor field with a continuous gauge freedom.

The constraints on the spatial variation of $\mathbf{m}_{\mathsf{E}}, \mathbf{m}_{\mathsf{T}_2}, \mathbf{m}_{\mathsf{T}_1-}$ may be obtained from the continuity of fields between A and B sublattice tetrahedra. The ground state constraints [Eq. (4)] in fact imply a set of *local* conservation laws, on the lattice. These conservation laws in turn suggest that a coarse-graining approach can be successful in describing the fluctuations of $\mathbf{m}_{\mathsf{E}}, \mathbf{m}_{\mathsf{T}_2}, \mathbf{m}_{\mathsf{T}_1-}$. And, unlike the global conservation laws

which underpin hydrodynamic theories, these fully local conservation laws can have consequences even for short wavelength fluctuations, as we shall see. Expanding the local constraints to leading order in a gradient expansion we find

$$\nabla \cdot \mathbf{m}_{\mathsf{T}_1-} = 0 \tag{5}$$

$$\begin{pmatrix} \partial_x m^1_{\mathsf{E}} \\ -\frac{1}{2}\partial_y m^1_{\mathsf{E}} + \frac{\sqrt{3}}{2}\partial_y m^2_{\mathsf{E}} \\ -\frac{1}{2}\partial_z m^1_{\mathsf{E}} - \frac{\sqrt{3}}{2}\partial_z m^2_{\mathsf{E}} \end{pmatrix} + \frac{\sqrt{3}}{2}\nabla \times \mathbf{m}_{\mathsf{T}_2} - \frac{3}{2}\sin(\phi'_{\mathsf{T}_1}) \begin{pmatrix} \partial_y m^z_{\mathsf{T}_1-} + \partial_z m^y_{\mathsf{T}_1-} \\ \partial_z m^x_{\mathsf{T}_1-} + \partial_x m^z_{\mathsf{T}_1-} \\ \partial_x m^y_{\mathsf{T}_1-} + \partial_y m^x_{\mathsf{T}_1-} \end{pmatrix} = 0 \tag{6}$$

where the angle ϕ'_{T_1} is a function of the exchange parameters, defined in the supplemental materials.

We wish to resolve the constraints (5)-(6) naturally using a gauge-theoretic approach. Note that since $\mathbf{m}_{\mathsf{T}_1-}$ appears in both constraints, we cannot simply introduce separate gauge fields to resolve Eqs. (5)-(6). Instead, we incorporate the eight components of $\{\mathbf{m}_{\mathsf{E}}, \mathbf{m}_{\mathsf{T}_2}, \mathbf{m}_{\mathsf{T}_1-}\}$ into a traceless tensor field $\mathcal{B}$:

$$\mathcal{B} = \begin{pmatrix} m^1_{\mathsf{E}} & -\frac{\sqrt{3}}{2}m^z_{\mathsf{T}_2} - \frac{3\sin(\phi'_{\mathsf{T}_1})}{2}m^z_{\mathsf{T}_1-} & \frac{\sqrt{3}}{2}m^y_{\mathsf{T}_2} - \frac{3\sin(\phi'_{\mathsf{T}_1})}{2}m^y_{\mathsf{T}_1-} \\ \frac{\sqrt{3}}{2}m^z_{\mathsf{T}_2} - \frac{3\sin(\phi'_{\mathsf{T}_1})}{2}m^z_{\mathsf{T}_1-} & -\frac{1}{2}m^1_{\mathsf{E}} + \frac{\sqrt{3}}{2}m^2_{\mathsf{E}} & -\frac{\sqrt{3}}{2}m^x_{\mathsf{T}_2} - \frac{3\sin(\phi'_{\mathsf{T}_1})}{2}m^x_{\mathsf{T}_1-} \\ -\frac{\sqrt{3}}{2}m^y_{\mathsf{T}_2} - \frac{3\sin(\phi'_{\mathsf{T}_1})}{2}m^y_{\mathsf{T}_1-} & \frac{\sqrt{3}}{2}m^x_{\mathsf{T}_2} - \frac{3\sin(\phi'_{\mathsf{T}_1})}{2}m^x_{\mathsf{T}_1-} & -\frac{1}{2}m^1_{\mathsf{E}} - \frac{\sqrt{3}}{2}m^2_{\mathsf{E}} \end{pmatrix} \tag{7}$$

Satisfaction of Eq. (6), along with the condition $\mathrm{Tr}[\mathcal{B}] = 0$ is guaranteed by the introduction of a symmetric, tensor field $\mathcal{Y}$ and writing

$$\mathcal{B} = \mathscr{D} \cdot \mathcal{Y}, \qquad \mathscr{D} \equiv \begin{pmatrix} 0 & -\partial_z & \partial_y \\ \partial_z & 0 & -\partial_x \\ -\partial_y & \partial_x & 0. \end{pmatrix} \tag{8}$$

The form of the matrix gauge field $\mathcal{Y}$ is then constrained by Eq. (5) which is satisfied if we take $\mathcal{Y}$ of the form

$$\mathcal{Y} = \begin{pmatrix} \psi & W_z & W_y \\ W_z & \psi & W_x \\ W_y & W_x & \psi \end{pmatrix}. \tag{9}$$

We can generate alternative forms of $\mathcal{Y}$ by applying Abelian gauge transformations to Eq. (9) of the form

$$\mathcal{Y}_{\mu\nu} \to \mathcal{Y}_{\mu\nu} + \partial_\mu \partial_\nu \zeta \tag{10}$$

The transformations of Eq. (10) leave the flux matrix $\mathcal{B}$, and therefore the physical spin system, unchanged. The form of $\mathcal{Y}$ in Eq. (9) thus corresponds to a specific choice of gauge. The theory of our spin liquid is therefore invariant under a group of gauge transformations $\zeta \in \mathbb{R}$. Abelian gauge transformations of a similar form to Eq. (10), acting on tensor fields also appear in the linearized theory of general relativity [19] and the theory of $S = 2$ gauge fields [20].

At low temperatures, where there are only fluctuations of the local fields $\mathbf{m}_{\mathsf{E}}, \mathbf{m}_{\mathsf{T}_2}, \mathbf{m}_{\mathsf{T}_1-}$, the free energy will be controlled by the entropy of these fluctuations. Coarse graining over some volume much larger than a unit cell but much smaller than the whole system, there will be more states available (and therefore more entropy) with small values of $\mathbf{m}_{\mathsf{E}}, \mathbf{m}_{\mathsf{T}_2}, \mathbf{m}_{\mathsf{T}_1-}$ [4]. The most general symmetry-allowed Gaussian free energy describing small fluctuations of these fields, when written in terms of the tensor field $\mathcal{Y}$, takes the form

$$\mathcal{F}_{\mathsf{SL}} = T \int \frac{d^3\mathbf{r}}{V_{\mathsf{u.c.}}} \Big[\lambda_{\mathsf{a}} \mathrm{Tr}[(\mathscr{D}\cdot\mathcal{Y})\cdot(\mathscr{D}\cdot\mathcal{Y})^T] + \lambda_{\mathsf{b}} \mathrm{Tr}[(\mathscr{D}\cdot\mathcal{Y})\cdot(\mathscr{D}\cdot\mathcal{Y})] + \lambda_{\mathsf{c}} \sum_\mu (\mathscr{D}\cdot\mathcal{Y})^2_{\mu\mu} \Big] \tag{11}$$

which is invariant under the gauge transformations of Eq. (10).

The distinctive nature of this spin liquid, and of the theory which describes it [Eq. (11)], can be revealed by neutron scattering experiments. This can be seen by calculating the correlation functions of the local fields $\mathbf{m}_{\mathsf{E}}, \mathbf{m}_{\mathsf{T}_2}, \mathbf{m}_{\mathsf{T}_1-}$ in momentum space. In addition to displaying pinch point singularities at zone centres, these correlation functions are singular approaching any momentum $\mathbf{q}$ which is along the (h,h,h) directions of reciprocal space, or along any direction related by the lattice symmetry to (h,h,h). This contrasts with the case of the Coulombic spin liquid which occurs in the case of spin ice, where the correlation functions are only singular at the Brillouin zone centre. Since the fields $\mathbf{m}_{\mathsf{E}}, \mathbf{m}_{\mathsf{T}_2}, \mathbf{m}_{\mathsf{T}_1-}$ are simply linear combinations of the spins, this singular behaviour will also show up in the spin structure factor $S(\mathbf{q})$, measurable in neutron scattering experiments.

In the vicinity of one of these singularities, at $T = 0$, the scattering is approximated by

$$S(\mathbf{K} + \mathbf{q}_\parallel + \mathbf{q}_\perp) \approx \sum_{\alpha\beta} \gamma_{\alpha\beta}(\mathbf{K}, \mathbf{q}_\parallel) \frac{q^\alpha_\perp q^\beta_\perp}{\mathbf{q}^2_\perp} \tag{12}$$

where $\mathbf{K}$ is a reciprocal lattice vector, $\mathbf{q}_\parallel$ is parallel to a $\langle 111 \rangle$

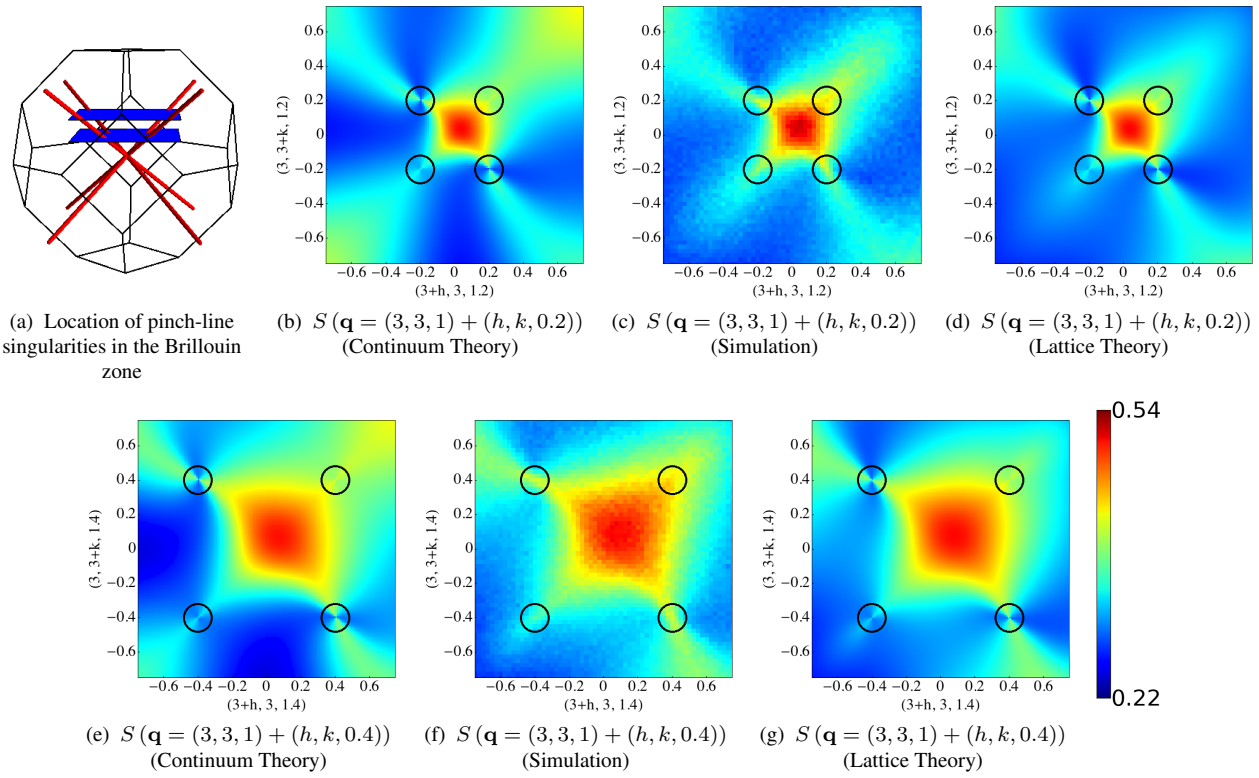

(a) Location of pinch-line singularities in the Brillouin zone

(b) $S(\mathbf{q} = (3,3,1) + (h,k,0.2))$ (Continuum Theory)

(c) $S(\mathbf{q} = (3,3,1) + (h,k,0.2))$ (Simulation)

(d) $S(\mathbf{q} = (3,3,1) + (h,k,0.2))$ (Lattice Theory)

(e) $S(\mathbf{q} = (3,3,1) + (h,k,0.4))$ (Continuum Theory)

(f) $S(\mathbf{q} = (3,3,1) + (h,k,0.4))$ (Simulation)

(g) $S(\mathbf{q} = (3,3,1) + (h,k,0.4))$ (Lattice Theory)

FIG. 3: **Gauge structure of the new spin liquid, as revealed through "pinch–line" singularities.** (a) Location of pinch–line singularities in reciprocal space. (b), (e) spin structure–factor $S(\mathbf{q})$ in parallel planes in reciprocal space in the Brillouin zone centred on $\mathbf{K} = (3,3,1)$, as calculated from the continuum theory [Eq. (11)]. Singular features are visible where these planes intersect $\langle 111 \rangle$ directions, as indicated by the black circles in each panel. These "pinch–line" singularities, Eq. (12), are characteristic of the gauge structure of the new spin liquid. (c), (f) spin structure factor calculated in finite temperature Monte Carlo simulation, in the same regions of reciprocal space. The pinch lines appear in the simulation results as sharp features around the point where $\langle 111 \rangle$ directions intersect the plane. (d), (g) a calculation of the structure factor made with a lattice based $1/\mathcal{N}$ theory, described in the supplemental material, also exhibiting pinch-line singularities. The simulations were performed at a temperature $T = 0.001$ K for a cluster of $N = 256000$ sites and dimensions $40a_0 \times 40a_0 \times 10a_0$ where a_0 is the linear size of a cubic unit cell. Results were calculated for parameters J_1=0.042, J_2=0.122, J_3=−0.118, J_4=−0.04 meV, with anisotropic g–tensor $g_\perp/g_\parallel$=1/3, in approximate correspondence to $Tb_2Ti_2O_7$ [25]. Since the crystal field ground state in $Tb_2Ti_2O_7$ is a non-Kramers doublet, the finite value of $g_\perp$ should be thought of as coming from mixing with the low lying crystal field excitation.

direction and $\mathbf{q}_\perp$ is orthogonal to that direction. The coefficients $\gamma_{\alpha\beta}$ determine the "orientation" of the singularity in $\mathbf{q}$-space. Their dependence on the Brillouin zone $\mathbf{K}$ may be thought of as a form factor determining the contribution of the fluctuations of each field $\mathbf{m}_\lambda$ to the scattering in each Brillouin zone. The dependence on $\mathbf{q}_\parallel$ is smooth and near a zone center $\mathbf{K}$ one may write $\gamma_{\alpha\beta}(\mathbf{K}, \mathbf{q}_\parallel) \approx \gamma_{\alpha\beta}(\mathbf{K}, \mathbf{0}) + \mathcal{O}(q_\parallel^2)$.

For $\gamma_{\alpha\beta} \not\propto \delta_{\alpha\beta}$ the structure factor in the limit $q_\perp \to 0$ will depend on the direction of approach and we have a singularity, along the entire $\langle 111 \rangle$ direction. Eq. (12) has the form of a pinch-point singularity extended into a line. We therefore will refer to it as a "pinch-line" singularity.

These "pinch lines" can be observed by taking planar cuts through scattering, which intersect these lines away from reciprocal lattice vectors [Fig. 3(a)]. This is illustrated using a $T = 0$ calculation of $S(\mathbf{q})$ from the gauge theory [Eq. (11)]] in Fig. 3(b), (e). For comparison, we show in Fig. 3(c), (f), the same quantity calculated at finite temperature within classical Monte Carlo simulation.

The simulation results show sharp features in the structure factor approaching the $\langle 111 \rangle$ directions, as predicted by the theory [Eq. (10)]. There is a small broadening of these singularities, coming from the finite temperature thermal fluctuations present in the Monte Carlo simulation. These features are even more clearly visible in the correlation functions of the local fields $\{\mathbf{m}_{\mathsf{E}}, \mathbf{m}_{\mathsf{T}_2}, m_{\mathsf{T}_1-}\}$, shown in the supplemental materials. The presence of the pinch lines in the simulation results is a strong validation of our theory of the spin liquid regime.

The continuum theory [Eq. (10)] was derived from local constraints, with associated local conservation laws, and the structure of the theory is inherited from the structure of those local constraints. This leads us to expect that the pinch-line singularities will be robust features of the spin liquid, even at short wavelengths. We have confirmed this expectation using two independent, lattice-based calculations. Firstly, the sharpening of the scattering around the $\langle 111 \rangle$ directions is clearly seen in the Monte Carlo simulations in Fig. 3(c), (f).

Secondly, we have also performed a $1/\mathcal{N}$ calculation of the spin correlations along the lines of that performed for the Heisenberg model in Ref. [21]. This calculation also predicts pinch-line singularities along the $\langle 111 \rangle$ directions of reciprocal space, as shown in Fig. 3(d), (g). It is therefore apparent that these singularities are a robust feature of the spin liquid, arising from the structure of its ground-state constraints, which is captured by the continuum theory derived in this Article.

Discussion

Thus far we have uncovered a spin liquid described by a tensor field carrying a continuous gauge symmetry, arising in a particular limit of a realistic model for magnetism on the pyrochlore lattice [Eq. (1)]. The signal feature of this spin liquid is sharp line-like singularities along $\langle 111 \rangle$ directions of reciprocal space, which occur in addition to pinch point singularities at zone centers. These "pinch-line" singularities are unique to the spin liquid discussed in this paper and as such provide a very discriminating "smoking gun" signature of this novel magnetic state. In the light of this discovery it is interesting to consider two known pyrochlore materials, which are often discussed in the context of spin liquid physics: $Tb_2Ti_2O_7$ and $Yb_2Ti_2O_7$.

$Tb_2Ti_2O_7$ has long been a focal point for discussion of 3-dimensional spin liquid physics [22–24]. While Eq. (1) alone may not constitute a complete quantitative model for the physics of $Tb_2Ti_2O_7$ it is interesting to compare observations on $Tb_2Ti_2O_7$ with the phenomenology of the spin liquid. Polarized neutron scattering experiments on $Tb_2Ti_2O_7$ have shown evidence of singular scattering at Brilllouin zone centers, but the form of this scattering looks rather different to a typical spin ice, especially in the non-spin flip (NSF) channel. At the same time, the data presented in Ref. 10, shows bright, narrow features extending along the $\langle 111 \rangle$ directions.

As a point of comparison to these experiments, the behaviour of the structure factor $S(\mathbf{q})$ in the spin flip (SF) and non spin flip (NSF) channels, appropriate to a polarised neutron scattering experiment with initial polarisation $\mathbf{n}||(1,-1,0)$, is shown in Fig. 1, for the same set of exchange parameters as in Fig. 3. Narrow prominences are visible in the SF channel along the $\langle 111 \rangle$ directions [Fig. 1(a)]. There are also pinch points in both channels at Brillouin zone centers. The distribution, orientation and polarisation dependence of the pinch points observed in [10] is the same as that in Fig. 1. In particular, we are able to reproduce the shape of the features in the NSF channel, something which cannot be done with a spin ice based description. The possibility that the theory described in this Article could apply to $Tb_2Ti_2O_7$ is lent weight by a recent attempt at parameterizing a pseudo-spin Hamiltonian for $Tb_{2+x}Ti_{2-x}O_{7+y}$ [26] which places it close to the three-way phase boundary at which this spin liquid emerges in our classical treatment.

Spin liquid behaviour at finite temperature does not rule out the possibility of an magnetic order at lower temperature. Indeed, recent experiments have demonstrated the presence of competing ordering phenomena in $Tb_2Ti_2O_7$, with quadrupolar [27, 28] and short range ordered antiferromagnetic states [11, 29, 30] being observed depending on the sample stoichiometry and experimental cooling protocol. This is consistent with the nature of the spin liquid considered in our manuscript, which sits at the confluence of many competing orders. In particular, we note that the ground-state manifold of the spin liquid contains states consistent with the $\mathbf{q}^* = (\pm 1/2, \pm 1/2, \pm 1/2)$ order observed under field cooled conditions [11, 29]. These states can only be connected to the other states of the spin liquid by rotation of an $\mathcal{O}(L)$ number of spins, where L is the linear size of the system. This may suggest an explanation for the sensitivity to how the system is cooled — namely that field cooling may drive the system into a state from which it is hard to reach the other parts of the ground state manifold.

The combination of spin liquid physics and prominent features in the scattering along $\mathbf{q} \parallel (1,1,1)$ is also strongly reminiscent of the discussion surrounding another pyrochlore: $Yb_2Ti_2O_7$ [31–35]. Indeed, it has recently been argued that the unusual physics of this material springs from competition between the E and T_1 regions of the phase diagram in Fig. 2(a) [15, 36]. In this context it is not unreasonable to imagine that the physics of the paramagnetic phase of $Yb_2Ti_2O_7$ may be influenced by a nearby spin liquid phase of the form described here. This provides an interesting alternative scenario to "quantum spin ice" physics in that material.

The theory presented in this Article provides a fundamentally different paradigm to the "emergent electromagnetism" known from spin ice and possesses a gauge freedom bearing an intriguing similarity to that appearing in the linearized theory of general relativity. This leads to the possibility of a unified theory of classical spin liquids on the pyrochlore lattice, and a classification of the above based on their associated gauge freedoms and the consequent singularities in their correlation functions. These issues will be explored further elsewhere.

The discovery of a new classical spin liquid is also a promising starting point for the discovery of new quantum spin liquid states [37, 38]. This possibility is exemplified by the quantum spin ice problem, in which introducing quantum fluctuations amongst the manifold of classical spin ice ground states leads to a quantum spin liquid with dynamic $U(1)$ gauge fields and fractionalized charges as excitations [38]. Indeed, the limit of perturbative quantum fluctuations around a classical spin ice is currently the only limit in which a quantum spin liquid is reliably predicted by a variety of theoretical methods in a realistic model for a pyrochlore magnet [39–44]. In the quantum spin ice case the classical and quantum limits of the problem are linked by a smooth thermal crossover [40, 44]. Similarly, studies of the quantum $S = 1/2$ Heisenberg model on the pyrochlore lattice find similar spin correlations [45–47] to those predicted by the gauge theoretic description of the classical problem [21]. We therefore expect that the classical results presented for the spin liquid discussed here are likely to remain relevant upon the inclusion of quantum fluctuations.

In conclusion, we have demonstrated the existence of a new classical spin liquid phase on the pyrochlore lattice, described by the fluctuations of a tensor field with a continuous gauge freedom. The unusual gauge structure is revealed by "pinch-line" singularities in correlations which could be observed in neutron scattering experiments.

Acknowledgements

This work was supported by the Theory of Quantum Matter Unit of the Okinawa Institute of Science and Technology Graduate University.

Author contributions

The analytic calculations were performed by O. B. and H. Y. The Monte Carlo simulations were written and performed by L. D. C. J. The manuscript was written by O. B. with input from all authors. N. S. supervised the project.

[1] Lee, P. A. & Nagaosa, N. Gauge theory of the normal state of high-T_c superconductors, *Phys. Rev. B* **46**, 5621-5639 (1992).

[2] Wen, X. G. Quantum orders and symmetric spin liquids, *Phys. Rev. B* **65**, 165113 (2002).

[3] Balents, L. Spin liquids in frustrated magnets, *Nature* **464**, 199-208 (2010).

[4] Henley, C. L. The "Coulomb phase" in frustrated systems, *Annu. Rev. Condens. Matter Phys.* **1**, 179-210 (2010).

[5] Gingras M. J. P. & McClarty, P. A. Quantum spin ice: a search for gapless quantum spin liquids in pyrochlore magnets, *Rep. Prog. Phys.* **77**, 056501 (2014).

[6] Castelnovo, C., Moessner, R. & Sondhi S. L. Magnetic monopoles in spin ice, *Nature* **451**, 42-45 (2008).

[7] Castelnovo, C., Moessner, R. & Sondhi S. L. Spin ice, fractionalization and topological order, *Annu. Rev. Condens. Matter Phys.* **3**, 35-55 (2012).

[8] Henley, C. L. Power-law spin correlations in pyrochlore antiferromagnets, *Phys. Rev. B* **71**, 014424 (2005).

[9] Fennell, T., Deen, P. P., Wildes, A. R., Schmalzl, K., Prabhakaran, D., Boothroyd, A. T., Aldus, R. J., McMorrow D. F. & Bramwell, S. T. Magnetic Coulomb phase in the spin ice $Ho_2Ti_2O_7$, *Science* **326**, 415-417 (2009).

[10] Fennell, T., Kenzelmann, M., Roessli, B., Haas, M. K. & Cava, R. J. Power-law spin correlations in the pyrochlore antiferromagnet $Tb_2Ti_2O_7$, *Phys. Rev. Lett.* **109**, 017201 (2012).

[11] Fritsch, K., Ross, K. A., Qiu, Y., Copley, J. R. D., Guidi, T., Bewley, R. I., Dabkowska, H. A. & Gaulin, B. D. Antiferromagnetic correlations at (1/2, 1/2, 1/2) in the ground state of the pyrochlore magnet $Tb_2Ti_2O_7$, *Phys. Rev. B* **87**, 094410 (2013).

[12] Guitteny S., Robert, J., Bonville, P., Ollivier, J., Decorse, C., Steffens, P., Boehm, M., Mutka, H., Mirebeau, I., & Petit, S. Anisotropic propagating excitations and quadrupolar effects in $Tb_2Ti_2O_7$, *Phys. Rev. Lett.* **111**, 087201 (2013).

[13] Curnoe, S.H., Quantum spin configurations in $Tb_2Ti_2O_7$, *Phys. Rev. B* **75**, 212404 (2007); *ibid.* **76**, 139903(E) (2007).

[14] Ross, K. A., Savary, L., Gaulin, B. D. & Balents, L. Quantum excitations in quantum spin ice, *Phys. Rev. X* **1**, 021002, (2011).

[15] Yan, H., Benton, O., Jaubert, L., & Shannon, N. Living on the edge: ground-state selection in quantum spin-ice pyrochlores, Preprint at http://arxiv.org/abs/1311.3501.

[16] Benton, O. Classical and quantum spin liquids on the pyrochlore lattice, PhD Thesis, University of Bristol (2015).

[17] McClarty, P., Curnoe, S. H., & Gingras, M. J. P. Energetic selection of ordered states in a model of the $Er_2Ti_2O_7$ frustrated pyrochlore XY antiferromagnet, *J. Phys.: Conf. Series* **145**, 012032, (2009).

[18] Jaubert, L. D. C., Harris, M. J., Fennell, T., Melko, R. G., Bramwell, S. T. & Holdsworth, P. C. W. Topological-sector fluctuations and Curie-law crossover in spin ice, *Phys. Rev. X* **3**, 011014 (2013).

[19] Misner, C. W., Thorne, K. S. & Wheeler, J. A. *Gravitation*, (W. H. Freeman, San Francisco, 1973).

[20] Fronsdal, C. Massless fields with integer spin, *Phys. Rev. D* **18**, 3624-3629, (1978).

[21] Isakov, S. V., Gregor, K., Moessner, R. & Sondhi, S. L. Dipolar Spin Correlations in Classical Pyrochlore Magnets, Phys. Rev. Lett. **93**, 167204 (2004).

[22] Gardner, J. S., Dunsiger, S. R., Gaulin, B. D., Gingras, M. J. P., Greedan, J. E., Kiefl, R. F., Lumsden, M. D., MacFarlane, W. A., Raju, N. P., Sonier, J. E., Swainson, I. & Tun, Z. Cooperative paramagnetism in the geometrically frustrated pyrochlore antiferromagnet in $Tb_2Ti_2O_7$, *Phys. Rev. Lett.* **82**, 1012-1015, (1999).

[23] Molavian, H. R., Gingras, M. J. P., & Canals, B. Dynamically induced frustration as a route to a quantum spin ice state in $Tb_2Ti_2O_7$ via virtual crystal field excitations and quantum many-body effects, *Phys. Rev. Lett.* **98**, 157204, (2007).

[24] Gardner, J. S., Gingras, M. J. P. & Greedan, J. E. Magnetic pyrochlore oxides, *Rev. Mod. Phys.* **82**, 53-107 (2010).

[25] Cao, H., Gukasov, A., Mirebeau, I., Bonville, P., Decorse, C. & Dhalenne, G. Ising versus XY anisotropy in frustrated $R_2Ti_2O_7$ compounds as "seen" by polarized neutrons, *Phys. Rev. Lett.* **103**, 056402 (2009).

[26] Takatsu, H., Kittaka, S., Kasahara, A., Kono, Y., Sakakibara, T., Kato, Y., Onoda, S., Fåk, B., Ollivier, J., Lynn, J. W., Taniguchi, T., Wakita, M. & Kadowaki, H., Quadrupole order in the frustrated pyrochlore $Tb_{2+x}Ti_{2-x}O_{7+y}$, Preprint at http://arxiv.org/abs/1506.04545 (2015).

[27] Taniguchi, T., Kadowaki, H., Takatsu, H., Fåk, B., Ollivier, J., Yamazaki, T., Sato, T. J., Yoshizawa, H., Shimura, Y., Sakakibara, T., Goto, K., Yaraskavitch, L. R. & Kycia, J. B., Long-range order and spin-liquid states of polycrystalline $Tb_{2+x}Ti_{2-x}O_{7+y}$, *Phys. Rev. B* **87**, 060408 (2013).

[28] Kadowaki, H., Takatsu, H., Taniguchi, T., Fåk, B., & Ollivier, J. Composite Spin and Quadrupole Wave in the Ordered Phase of $Tb_{2+x}Ti_{2-x}O_{7+y}$, *Spin* **5**, 1540003 (2015).

[29] Kermarrec, E., Maharaj, D. D., Gaudet, J., Fritsch, K., Pomaranski, D., Kycia, J. B., Qiu, Y., Copley, J. R. D., Couchman, M., Morningstar, M., Dabkowska, H. A. & Gaulin, B. D. Gapped and gapless short range ordered magnetic states with $(\frac{1}{2}, \frac{1}{2}, \frac{1}{2})$ wavectors in the pyrochlore magnet $Tb_{2+x}Ti_{2-x}O_{7+\delta}$, *Phys. Rev. B* **92**, 245114, (2015).

[30] Guitteny, S., Mirebeau, I., de Reotier, P. D., Colin, C. V., Bonville, P., Porcher, F., Grenier, B., Decorse, C. & Petit, S., Mesoscopic correlations in $Tb_2Ti_2O_7$, *Phys. Rev. B* **92**, 144412, (2015).

[31] Bonville, P., Hodges, J. A., Bertin, E., Bouchaud, J.-P., Dalmas de Reotier, P., Regnault, L.-P., Ronnow, H. M., Sanchez, J.-P., Sosin, S. & Yaouanc, A. Transitions and spin dynamics at very low temperature in the pyrochlores $Yb_2Ti_2O_7$ and $Gd_2Sn_2O_7$, *Hyperfine Interact.* **156/157**, 103-111 (2004).

[32] Ross, K. A., Ruff, J. P. C., Adams, C. P., Gardner, J. S., Dabkowska, H. A., Qiu, Y., Copley, J. R. D., & Gaulin, B. D. Two-dimensional kagome correlations and field induced order

in the ferromagnetic XY pyrochlore $Yb_2Ti_2O_7$, *Phys. Rev. Lett.* **103**, 227202 (2009).

[33] Thompson, J. D., McClarty, P. A., Ronnow, H. M., Regnault, L. P., Sorge, A., & Gingras, M. J. P. Rods of neutron scattering intensity in $Yb_2Ti_2O_7$: compelling evidence for significant anisotropic exchange in a magnetic pyrochlore oxide, *Phys. Rev. Lett.* **106**, 187202 (2011).

[34] Chang, L. J., Onoda, S., Su, Y., Kao, Y.-J., Tsuei, K.-D., Yasui, Y., Kakurai, K. & Lees, M. R. Higgs transition from a magnetic Coulomb liquid to a ferromagnet in $Yb_2Ti_2O_7$, *Nature Commun.* **3**, 992, (2012).

[35] Yaouanc, A., Maisuradze, A., & Dalmas de Réotier, P. Influence of short range correlations on the μSR polarization functions in the slow dynamic limit: application to the quantum spin-liquid system $Yb_2Ti_2O_7$, *Phys. Rev. B* **87**, 134405 (2013).

[36] Jaubert, L.D.C., Benton, O., Rau, J. G., Oitmaa, J., Singh, R. R. P., Shannon, N. & Gingras, M. J. P. Are multiphase competition & order-by-disorder the keys to understanding $Yb_2Ti_2O_7$?, *Phys. Rev. Lett.* **115**, 267208, (2015).

[37] Moessner, R. & Sondhi, S. L. Three-dimensional resonating-valence-bond liquids and their excitations, *Phys. Rev. B* **68**, 064411, (2003).

[38] Hermele, M., Fisher, M. P. A. & Balents, L. Pyrochlore photons: The U(1) spin liquid in a S=1/2 three-dimensional frustrated magnet, *Phys. Rev. B* **69**, 064404 (2004).

[39] Banerjee, A., Isakov, S. V., Damle, K. & Kim, Y.-B. Unusual liquid state of hard-core bosons on the pyrochlore lattice, *Phys. Rev. Lett.* **100**, 047208 (2008).

[40] Benton, O., Sikora, O. & Shannon, N. Seeing the light: Experimental signatures of emergent electromagnetism in a quantum spin ice, *Phys. Rev. B* **86**, 075154 (2012).

[41] Shannon, N., Sikora, O., Pollmann, F., Penc, K. & Fulde, P. Quantum ice: A quantum Monte Carlo study, *Phys. Rev. Lett.* **108**, 067204 (2012).

[42] Savary, L. & Balents, L. Coulombic quantum liquids in spin-1/2 pyrochlores, *Phys. Rev. Lett.* **108**, 037202 (2012).

[43] Hao, Z., Day, A. G. R. and Gingras, M. J. P. Bosonic many-body theory of quantum spin ice, *Phys. Rev. B* **88**, 144402 (2014).

[44] Kato, Y. & Onoda, S. Numerical evidence of quantum melting of spin ice: quantum-to-classical crossover, *Phys. Rev. Lett.* **115**, 077202 (2015).

[45] Canals, B. & Lacroix, C. Pyrochlore Antiferromagnet: A Three-Dimensional Quantum Spin Liquid, *Phys. Rev. Lett.* **80**, 2933-2936 (1998)

[46] Canals, B. and Lacroix, C. Quantum spin liquid: The Heisenberg antiferromagnet on the three-dimensional pyrochlore lattice, *Phys. Rev. B* **61**, 1149 (2000)

[47] Huang, Y., Chen, K., Deng, Y., Prokof'ev, N. & Svistunov, B. Spin-Ice State of the Quantum Heisenberg Antiferromagnet on the Pyrochlore Lattice, Preprint at http://arxiv.org/abs/1511.08285.

From pinch points to pinch lines: a new spin liquid on the pyrochlore lattice– supplemental material

Owen Benton,[1] Ludovic Jaubert,[1] Han Yan,[1] and Nic Shannon[1]

[1] *Okinawa Institute of Science and Technology Graduate University, Onna-son, Okinawa 904-0395, Japan*

DEFINITION OF LOCAL FIELDS AND SUSCEPTIBILITIES

It was shown in [1] that the generalized model for nearest neighbour exchange on the pyrochlore lattice [Eq. (1) of the main text] may be exactly rewritten in terms of local fields, defined on the pyrchlore tetrahedra

$$\mathcal{H}_{\mathsf{ex}} = \frac{1}{2}\sum_{\mathsf{tet}} \left(\Delta_{\mathsf{A}_2} m_{\mathsf{A}_2}^2 + \Delta_{\mathsf{E}} \mathbf{m}_{\mathsf{E}}^2 + \Delta_{\mathsf{T}_2} \mathbf{m}_{\mathsf{T}_2}^2 + \Delta_{\mathsf{T}_1 +} \mathbf{m}_{\mathsf{T}_1 +}^2 + \Delta_{\mathsf{T}_1 -} \mathbf{m}_{\mathsf{T}_1 -}^2 \right) + \text{constant}. \tag{1}$$

The fields are labelled by the irreducible representations of the point group according to which they transform. These fields are defined in Table I.

Local OP	Definition in terms of spins
m_{A_2}	$\frac{1}{\sqrt{3}}\left(S_0^x + S_0^y + S_0^z + S_1^x - S_1^y - S_1^z - S_2^x + S_2^y - S_2^z - S_3^x - S_3^y + S_3^z\right)$
$\mathbf{m}_{\mathsf{E}}$	$\begin{pmatrix} \frac{1}{\sqrt{6}}\left(-2S_0^x + S_0^y + S_0^z - 2S_1^x - S_1^y - S_1^z + 2S_2^x + S_2^y - S_2^z + 2S_3^x - S_3^y + S_3^z\right) \\ \frac{1}{\sqrt{2}}\left(-S_0^y + S_0^z + S_1^y - S_1^z - S_2^y - S_2^z + S_3^y + S_3^z\right) \end{pmatrix}$
$\mathbf{m}_{\mathsf{T}_2}$	$\begin{pmatrix} \frac{1}{\sqrt{2}}\left(-S_0^y + S_0^z + S_1^y - S_1^z + S_2^y + S_2^z - S_3^y - S_3^z\right) \\ \frac{1}{\sqrt{2}}\left(S_0^x - S_0^z - S_1^x - S_1^z - S_2^x + S_2^z + S_3^x + S_3^z\right) \\ \frac{1}{\sqrt{2}}\left(-S_0^x + S_0^y + S_1^x + S_1^y - S_2^x - S_2^y + S_3^x - S_3^y\right) \end{pmatrix}$
$\mathbf{m}_{\mathsf{T}_{1,\mathsf{ice}}}$	$\begin{pmatrix} \frac{1}{\sqrt{3}}(S_0^x + S_0^y + S_0^z + S_1^x - S_1^y - S_1^z + S_2^x - S_2^y + S_2^z + S_3^x + S_3^y - S_3^z) \\ \frac{1}{\sqrt{3}}(S_0^x + S_0^y + S_0^z - S_1^x + S_1^y + S_1^z - S_2^x + S_2^y - S_2^z + S_3^x + S_3^y - S_3^z) \\ \frac{1}{\sqrt{3}}(S_0^x + S_0^y + S_0^z - S_1^x + S_1^y + S_1^z + S_2^x - S_2^y + S_2^z - S_3^x - S_3^y + S_3^z) \end{pmatrix}$
$\mathbf{m}_{\mathsf{T}_{1,\mathsf{planar}}}$	$\begin{pmatrix} \frac{1}{\sqrt{6}}(-2S_0^x + S_0^y + S_0^z - 2S_1^x - S_1^y - S_1^z - 2S_2^x - S_2^y + S_2^z - 2S_3^x + S_3^y - S_3^z) \\ \frac{1}{\sqrt{6}}(S_0^x - 2S_0^y + S_0^z - S_1^x - 2S_1^y + S_1^z - S_2^x - 2S_2^y - S_2^z + S_3^x - 2S_3^y - S_3^z) \\ \frac{1}{\sqrt{6}}(S_0^x + S_0^y - 2S_0^z - S_1^x + S_1^y - 2S_1^z + S_2^x - S_2^y - 2S_2^z - S_3^x - S_3^y - 2S_3^z) \end{pmatrix}$
$\mathbf{m}_{\mathsf{T}_1 -}$	$\cos(\phi'_{\mathsf{T}_1})\mathbf{m}_{\mathsf{T}_1\mathsf{ice}} + \sin(\phi'_{\mathsf{T}_1})\mathbf{m}_{\mathsf{T}_1\mathsf{planar}}$
$\mathbf{m}_{\mathsf{T}_{1,+}}$	$-\sin(\phi'_{\mathsf{T}_1})\mathbf{m}_{\mathsf{T}_1\mathsf{ice}} + \cos(\phi'_{\mathsf{T}_1})\mathbf{m}_{\mathsf{T}_1\mathsf{planar}}$

TABLE I: Definition of the local fields $\mathbf{m}_\lambda$ appearing in Eq. (1). The exchange Hamiltonian $\mathcal{H}_{\mathsf{ex}}$ [Eq. (1) of the main text] reduces to a sum of quadratic forms when written in terms of these fields [1]. The labels $\mathsf{A}_2, \mathsf{E}, \mathsf{T}_2, \mathsf{T}_1$ refer to the irreducible representation of the point group according to which the corresponding field transforms. There are two fields which transform according to the T_1 irrep. The parameter ϕ'_{T_1} is chosen as a function of the exchange parameters to remove the symmetry allowed coupling between these fields.

The angle ϕ'_{T_1} which appears in the definitions of $\mathbf{m}_{\mathsf{T}_1+}$ and $\mathbf{m}_{\mathsf{T}_1-}$ is chosen such that there is no bilinear coupling between $\mathbf{m}_{\mathsf{T}_1+}$ and $\mathbf{m}_{\mathsf{T}_1-}$ and such that

$$a_{\mathsf{T}_1-} \leq a_{\mathsf{T}_1+}. \tag{2}$$

Note that this convention for the definition of the T_1 symmetric fields is dfifferent to that chosen in Ref. [1].

Following common practice in Monte Carlo simulations, the order parameter susceptibilities appearing in Fig. 2 of the main text are calculated in according to the following formula:

$$\chi = \frac{N}{T}\left(\langle \mathbf{m}_\lambda^2 \rangle - \langle |\mathbf{m}_\lambda| \rangle^2\right) \tag{3}$$

where N is the number of spins in the system, T is the temperature and $\mathbf{m}_\lambda$ are the local fields given in Table I.

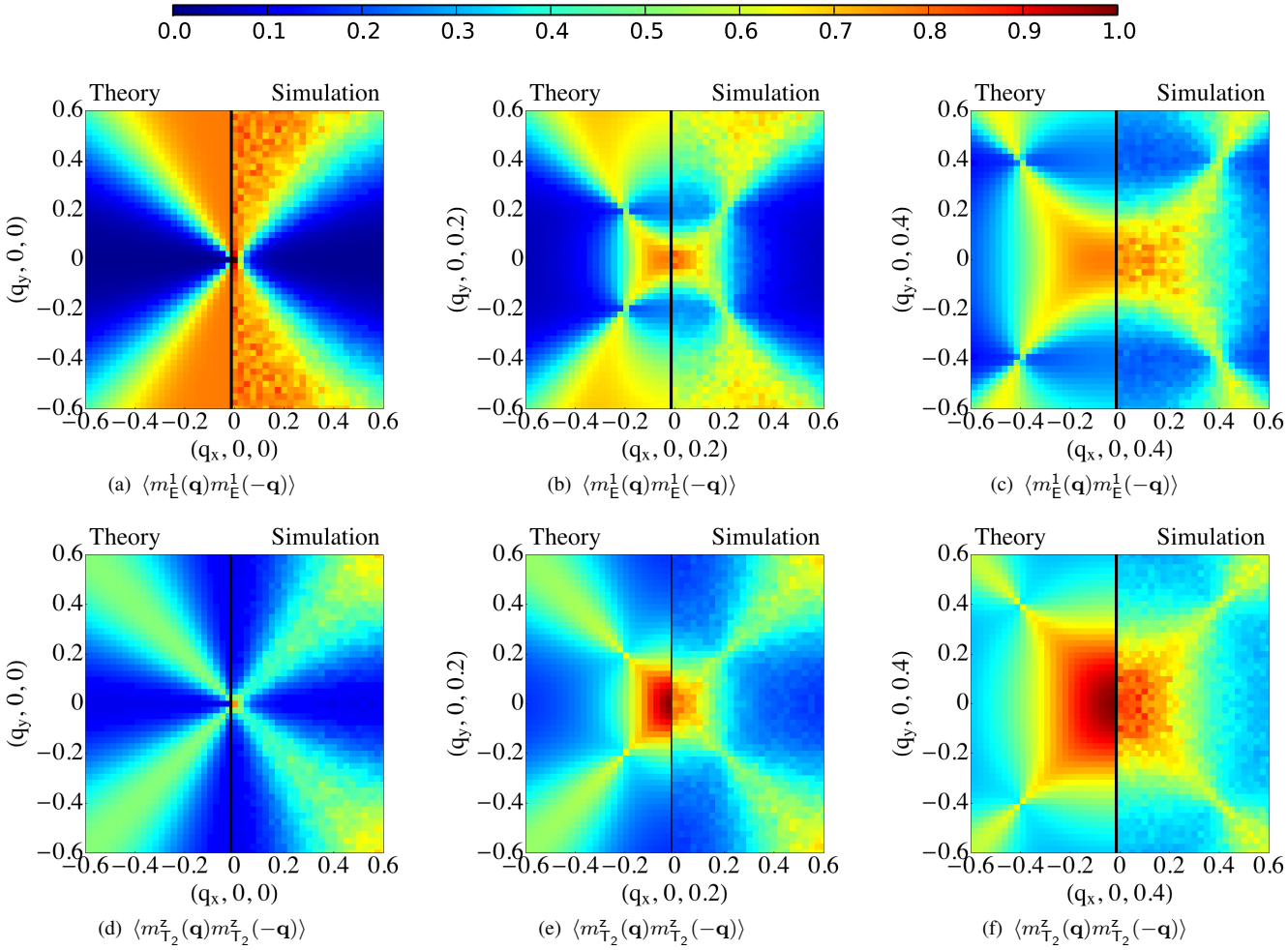

(a) $\langle m^1_{\mathsf{E}}(\mathbf{q}) m^1_{\mathsf{E}}(-\mathbf{q})\rangle$ (b) $\langle m^1_{\mathsf{E}}(\mathbf{q}) m^1_{\mathsf{E}}(-\mathbf{q})\rangle$ (c) $\langle m^1_{\mathsf{E}}(\mathbf{q}) m^1_{\mathsf{E}}(-\mathbf{q})\rangle$

(d) $\langle m^z_{\mathsf{T}_2}(\mathbf{q}) m^z_{\mathsf{T}_2}(-\mathbf{q})\rangle$ (e) $\langle m^z_{\mathsf{T}_2}(\mathbf{q}) m^z_{\mathsf{T}_2}(-\mathbf{q})\rangle$ (f) $\langle m^z_{\mathsf{T}_2}(\mathbf{q}) m^z_{\mathsf{T}_2}(-\mathbf{q})\rangle$

FIG. 1: Comparison of the correlation functions $\langle m^1_{\mathsf{E}}(\mathbf{q}) m^1_{\mathsf{E}}(-\mathbf{q})\rangle$, $\langle m^z_{\mathsf{T}_2}(\mathbf{q}) m^z_{\mathsf{T}_2}(-\mathbf{q})\rangle$ as calculated in the continuum field theory (left half of panels) and Monte Carlo simulation (right half of panels) of a cluster of $N = 256000$ spins at temperature $T = 0.001$ K. The field theory calculation is shown on a discrete grid in momentum space for the sake of comparison with the simulations which are carried out on a finite lattice with linear dimensions $L_x \times L_y \times L_z = 40 \times 40 \times 10\ a_0^3$ with periodic boundary conditions, where a_0 is the linear dimension of a cubic unit cell. The singular features found in simulation are exactly reproduced by the continuum theory [Eq. (11) of main text], with pinch-line singularities visible in both calculations where the planes of scattering cut the $\langle 111\rangle$ directions. Calculations are carried out for the set of exchange parameters J_1=0.042, J_2=0.122, J_3=−0.118, J_4=−0.04 meV, as in Fig. 3 of the mauscript.

CORRELATION FUNCTIONS OF THE FIELDS $\mathbf{m}_\lambda$

In Figs. 1 we show examples of the momentum space correlation functions of the local fields $\{\mathbf{m}_{\mathsf{E}}, \mathbf{m}_{\mathsf{T}_2}, \mathbf{m}_{\mathsf{T}_1-}\}$, as calculated from the continuum theory developed in the manuscript (left half of panels) and from Monte Carlo simulation (right half of panels). Specifically, we show the correlation functions

$$\langle m_{\mathsf{E}}(\mathbf{q})^1 m_{\mathsf{E}}(-\mathbf{q})^1\rangle, \quad \langle m_{\mathsf{T}_2}(\mathbf{q})^z m_{\mathsf{T}_2}(-\mathbf{q})^z\rangle,$$

in three planes of reciprocal space

$$\mathbf{q} = \frac{2\pi}{a_0}(h,k,0), \quad \mathbf{q} = \frac{2\pi}{a_0}(h,k,0.2), \quad \mathbf{q} = \frac{2\pi}{a_0}(h,k,0.4)$$

in each case we see singular features wherever the planes cut the $\langle 111\rangle$ directions.

The Fourier transforms of the local fields are defined as

$$m^\gamma_\alpha(\mathbf{q}) = \sqrt{\frac{1}{N_{\text{u.c.}}}} \sum_{\text{tet}\in\text{A}} \exp[-i\mathbf{q}\cdot\mathbf{r}_{\text{tet}}] m^\gamma_\alpha(\mathbf{r}_{\text{tet}}) \tag{4}$$

where $N_{\mathsf{u.c.}}$ is the number of unit cells, the sum runs over only the 'A' sublattice of tetrahedra and $\mathbf{r}_{\mathsf{tet}}$ are the positions of the centers of those tetrahedra.

The correlation functions agree well between the continuum theory and simulation. The qualitative structure of the correlations is in agreement for all cases, although some quantitative differences are visible at shorter wavelengths. Most importantly, the Monte Carlo simulations clearly show the sharpening of the correlation functions approaching the $\langle 111 \rangle$ directions, as predicted by the field theory, demonstrating that the pinch lines are a robust feature of the spin liquid regime.

LATTICE BASED CALCULATION OF THE CORRELATIONS IN THE SPIN-LIQUID REGIME

For the purposes of comparison with the continuum, we have also performed some fully lattice based calculations of the correlations in the spin liquid regime.

These calculations follow a method which has been previously been shown successful in understanding the correlations of disordered phases of the Heisenberg model on the pyrochlore lattice [2], spin ice [3] and protons in water ice [4].

In this approach the constraints on the lengths of the spins

$$\mathbf{S}_i^2 = S^2 \tag{5}$$

are only enforced on average

$$\langle \mathbf{S}_i^2 \rangle = S^2. \tag{6}$$

Eq. (6) is enforced by means of a Lagrange multiplier λ added to the Hamiltonian. We write

$$\beta H \rightarrow \beta H_\lambda = \beta H + \lambda \sum_i \mathbf{S}_i^2 \tag{7}$$

where β is the inverse temperature.

Using a Fourier transformation βH_λ may be written as

$$\beta H_\lambda = \frac{1}{2} \tilde{S}(-\mathbf{q}) \cdot \mathcal{M}(\mathbf{q}) \cdot \tilde{S}(\mathbf{q}) \tag{8}$$

where is $\tilde{S}(\mathbf{q})$ is a 12-component vector formed from the Fourier transforms of the 3 spin components on each of the 4 sublattices.

The correlations of $\tilde{S}(\mathbf{q})$ are then

$$\langle \tilde{S}_i(-\mathbf{q}) \tilde{S}_j(\mathbf{q}) \rangle = (\mathcal{M}^{-1}(\mathbf{q}))_{ij} \tag{9}$$

and λ can be chosen such that Eq. (6) is obeyed.

Where $\mathcal{M}(\mathbf{q})$ possesses flat bands of eigenvalues at the bottom of its spectrum- as is the case in the spin liquid regime- the limit $T \rightarrow 0$ of the correlation function becomes a projection matrix, projecting into the subspace described by the associated eigenvectors [4]. This projection operator can be thought of as enforcing the local ground state constraints [3].

It is this, zero temperature limit of the correlation function which is plotted in Figs. 3(d) and 3(g) of the main text.

The approach outlined here can be constructed as a pertubative expansion in powers of $1/\mathcal{N}$, where $\mathcal{N}$ is a number of copies of the system and the spin length constraint [Eq. (6)] becomes

$$\frac{1}{\mathcal{N}} \sum_{\alpha=1}^{\mathcal{N}} \mathbf{S}_{i,\alpha}^2 = S^2 \tag{10}$$

This method is described in more detail in Ref. [5].

[1] Yan, H., Benton, O., Jaubert, L., and Shannon, N., Living on the edge: ground-state selection in quantum spin-ice pyrochlores, Preprint at http://arxiv.org/abs/1311.3501.

[2] Isakov, S. V., Gregor, K., Moessner, R. and Sondhi, S. L., Dipolar Spin Correlations in Classical Pyrochlore Magnets, *Phys. Rev. Lett.* **93**, 167204, (2004).

[3] Henley, C. L., Power-law spin correlations in pyrochlore antiferromagnets, *Phys. Rev. B* **71**, 014424 (2005).

[4] Isakov, S. V., Moessner, R., Sondhi, S. L. and Tennant, D. A., Analytical theory for proton correlations in common-water ice I_h, *Phys. Rev. B* **91**, 245152 (2015).

[5] Benton, O. Classical and quantum spin liquids on the pyrochlore lattice, PhD Thesis, University of Bristol (2015).